A Hidden Markov Model for 3D Catheter Tip Tracking with 2D X-ray Catheterization Sequence and 3D Rotational Angiography

Ambrosini, Pierre; Smal, Ihor; Ruijters, Daniel; Niessen, Wiro J.; Moelker, Adriaan; Van Walsum, Theo

DOI
10.1109/TMI.2016.2625811

Publication date
2017

Document Version
Final published version

Published in
IEEE Transactions on Medical Imaging

A Hidden Markov Model for 3D Catheter Tip Tracking With 2D X-ray Catheterization Sequence and 3D Rotational Angiography

Pierre Ambrosini,* Ihor Smal, Daniel Ruijters, Wiro J. Niessen, Adriaan Moelker, and Theo Van Walsum

***Abstract*— In minimal invasive image guided catheterization procedures, physicians require information of the catheter position with respect to the patient's vasculature. However, in fluoroscopic images, visualization of the vasculature requires toxic contrast agent. Static vasculature roadmapping, which can reduce the usage of iodine contrast, is hampered by the breathing motion in abdominal catheterization. In this paper, we propose a method to track the catheter tip inside the patient's 3D vessel tree using intra-operative single-plane 2D X-ray image sequences and a peri-operative 3D rotational angiography (3DRA). The method is based on a hidden Markov model (HMM) where states of the model are the possible positions of the catheter tip inside the 3D vessel tree. The transitions from state to state model the probabilities for the catheter tip to move from one position to another. The HMM is updated following the observation scores, based on the registration between the 2D catheter centerline extracted from the 2D X-ray image, and the 2D projection of 3D vessel tree centerline extracted from the 3DRA. The method is extensively evaluated on simulated and clinical datasets acquired during liver abdominal catheterization. The evaluations show a median 3D tip tracking error of 2.3 mm with optimal settings in simulated data. The registered vessels close to the tip have a median distance error of 4.7 mm with angiographic data and optimal settings. Such accuracy is sufficient to help the physicians with an up-to-date roadmapping. The method tracks in real-time the catheter tip and enables roadmapping during catheterization procedures.**

***Index Terms*— 3DRA, abdominal, breathing, catheter, catheterization, fluoroscopy, guidance, hidden Markov Model, liver, rigid, registration, TACE, tip, tracking, X-ray.**

I. Introduction

NOWADAYS, minimally invasive procedures are common because of the associated benefits for the patients, such as shorter recovery times. For example, catheterization procedures are executed to non-invasively reach locations via the vasculature. During catheterization, image guidance is commonly performed using intra-operative 2D X-ray fluoroscopy. On this imaging modality, the catheter is visible but the vasculature is not. Physicians need to know where the catheter (particularly the tip) is to navigate to a specific target. To this end, 2D intra-operative images are conventionally enhanced using contrast agent to visualize the vasculature, which permits physicians to localize the catheter inside the vasculature. However, contrast agent cannot be used continuously due to its toxicity. Also, the projected vasculature can sometimes be difficult to interpret. To have a continuous roadmap, physicians use 2D overlays of Digital Subtraction Angiography (DSA) onto the X-ray images. 3D projection overlays, e.g. from pre-operative CTA or MR images, have also been used [1]. Unfortunately, such 2D and 3D roadmaps are generally static and the registration between 3D vasculature extracted from CTA/MRA and 2D images is not straightforward. In e.g. abdominal catheterization, respiration induced motion and the catheter stiffness lead to motion and deformation of the vasculature, invalidating the roadmap.

The purpose of our work is to continuously localize the catheter tip inside the 3D model of the patients vasculature during the catheterization procedures. The paper focuses particularly on liver catheterization interventions such as Transcatheter Arterial Chemoembolization (TACE). We propose a method to track the catheter tip inside a patient-specific contrast-enhanced 3D abdominal vasculature, obtained from peri-operative 3D Rotational Angiography (3DRA), using single-plane 2D X-ray images with no contrast agent. The proposed tip tracking method enables 2D as well as 3D roadmapping that can easily be integrated in the intervention and permits continuous and contrast-free image guidance (Fig. 1). Such image guidance would potentially reduce toxic contrast agent use and may decrease procedure time as well. In liver catheterization, peri-interventional 3DRA (which is a form of Cone Beam Computed Tomography, CBCT) is acquired at the beginning of the procedure when the catheter is in the

Manuscript received August 29, 2016; revised October 30, 2016; accepted October 31, 2016. Date of publication November 7, 2016; date of current version March 2, 2017. This research was funded by Philips Healthcare, Best, The Netherlands. *Asterisk indicates corresponding author.*

*P. Ambrosini is with the Biomedical Imaging Group Rotterdam, the Department of Radiology & Nuclear Medicine and the Department of Medical Informatics, Erasmus MC, University Medical Center Rotterdam, 3000 CA Rotterdam, The Netherlands (e-mail: p.ambrosini@erasmusmc.nl).

I. Smal and T. Van Walsum are with the Biomedical Imaging Group Rotterdam, Department of Radiology & Nuclear Medicine and the Department of Medical Informatics, Erasmus MC, University Medical Center Rotterdam, 3000 CA Rotterdam, The Netherlands.

D. Ruijters is with Image Guided Therapy Systems Innovation, Philips Healthcare, 5680 DA Best, The Netherlands.

W. J. Niessen is with the Biomedical Imaging Group Rotterdam, Department of Radiology & Nuclear Medicine and the Department of Medical Informatics, Erasmus MC, University Medical Center Rotterdam, 3000 CA Rotterdam, The Netherlands and also with the Imaging Science and Technology, Faculty of Applied Sciences, Delft University of Technology, 2628 CD Delft, The Netherlands.

A. Moelker is with the Department of Radiology & Nuclear Medicine, Erasmus MC, University Medical Center Rotterdam, 3000 CA Rotterdam, The Netherlands.

Digital Object Identifier 10.1109/TMI.2016.2625811

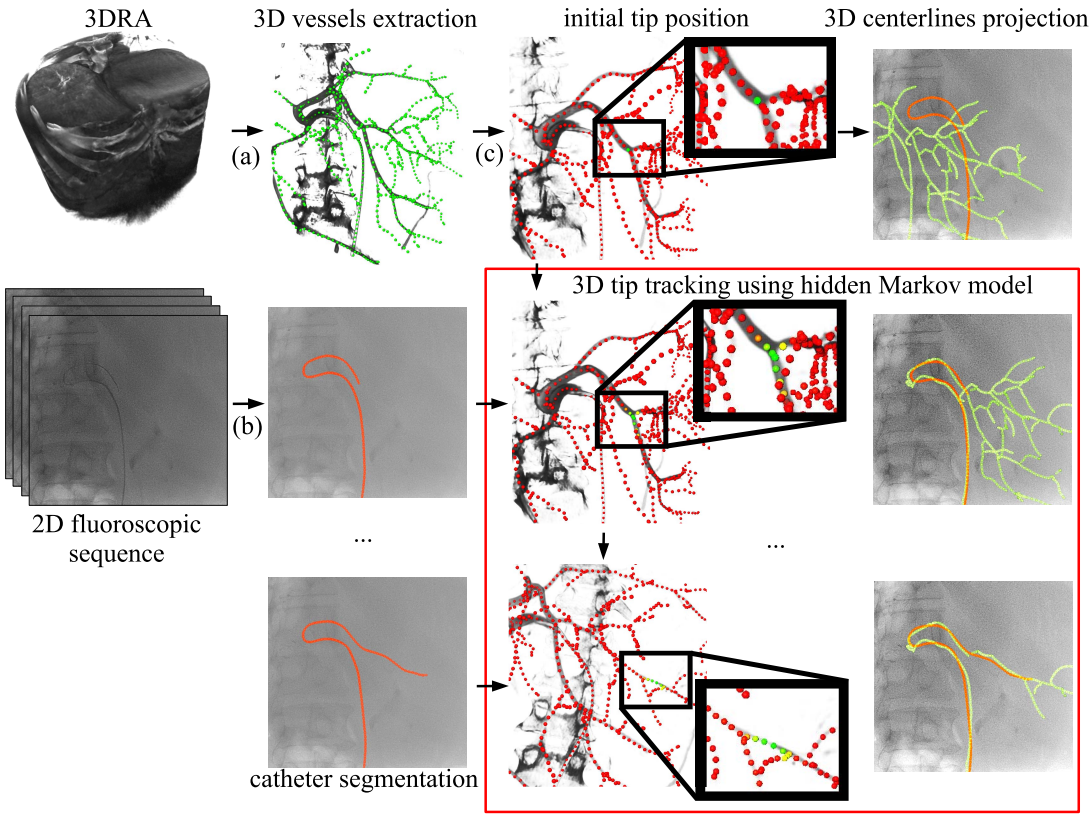

Fig. 1. Tip tracking workflow: (a) 3D vessel tree is extracted from 3DRA. (a) 2D catheter is extracted for each frame of the X-ray sequence. (a) The HMM is initialized with the initial tip position in the 3D vessel tree. The HMM is then updated depending on the 3D/2D registration metric. The tip position and the registered transformation are obtained which can be used as a 3D/2D roadmap to guide the physician. The tracking using HMM (red frame) is the scope of this paper. The other steps are approached in the discussion.

common hepatic artery. The contrast agent is injected directly into the liver vessels to offer a better visibility of the vascular morphology. 3DRA provides a better understanding of the vasculature compared to DSA because of its 3D nature. It also helps to position the C-arm to obtain an optimal view on the vessels, taking foreshortening, overlap and bifurcations into account. 3DRA is more and more acquired during TACE procedure because it increases the confidence of the physician and it helps for the planning and the guidance [2].

Most current approaches in image guidance for catheterization procedures focus on registering a 3D pre-operative angiographic image, such as CTA or MRA, with intra-operative 2D images, such as single-plane/bi-plane X-ray images or DSA. Thorough reviews of 3D/2D registration methods have been presented by Markelj et al. [3] and Liao et al. [4]. Various methods have been proposed for cardiac [5]–[9], cranial [10]–[13] and abdominal [14]–[16] procedures. These methods use the image intensity, gradient or features such as bones and more generally vessels, to spatially align the 3D image to the 2D image. In cardiac and abdominal procedures, due to respiratory motion, the registration has to be updated continuously. Methods that utilize vessel information for alignment can not be used continuously, as the vessels are not continuously visible because of the contrast agent toxicity. Ambrosini et al. [17], Atasoy et al. [18] and Ma et al. [19] correct for breathing motion using other features in the 2D X-ray image such as diaphragm/heart border, tracheal bifurcation or the catheter. The use of such features gives reasonably accurate results but the robustness depends on the complete visibility of the features. In abdominal X-ray catheterization images, only the catheter is visible and the catheter-based registration fails if the visible catheter part is too short [17]. Using the catheter-based registration combined with a hidden Markov model (HMM) [20], our feasibility study [21] showed that 3D catheter tip tracking over the time was possible and could potentially overcome the problem of short feature visibility such as short part of the catheter visible on 2D X-ray images. This study was limited but showed encouraging results for 3D/2D roadmapping in abdominal catheterization procedures.

This paper has two main contributions. First, we present a novel and robust 3D catheter tip tracking method, based on an HMM, and that extends our previous preliminary work [21]. We propose a new transition probability between the states in the HMM. Furthermore, a new cost function and different initialization is introduced for the 3D/2D registration. Second, we perform extensive quantitative and qualitative evaluations with both simulated and clinical data, using clinically relevant measures, i.e. tip distance error and vessel distance error close to the tip. In summary, this method presents the following advancements compared to the state of the art:

- The tip tracking as well as the roadmapping can be performed continuously using fluoroscopic imaging without the need for contrast agent and with no distinctive features except the catheter,

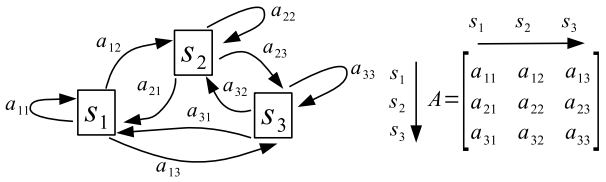

Fig. 2. HMM with 3 states and its matrix A of state transition probabilities.

- 3D roadmapping is provided next to 2D roadmapping. This would add more information for the physician with difficult cases,
- The nature of the tracking method provides temporal consistency of the tracking results, and as such is robust to e.g. field-of-view changes.

II. Method

The purpose of our method is to track the catheter tip inside the 3D vessel tree extracted from the peri-operative 3DRA using information from 2D fluoroscopic imaging. A probability distribution of the 3D catheter tip position is computed using an HMM. The probability distribution update is based on the previous distribution and the 3D/2D registration results of the 3D vessel tree and the 2D catheter centerline extracted from the 2D intra-operative X-ray image. In this process, a 3D/2D registration is performed for the most probable catheter tip locations.

In the following, we first describe the HMM that was used and then show how it applies to our application with the catheter tip tracking.

A. Hidden Markov Model

A hidden Markov model is a system with a set of N states $S = \{s_1, \dots s_N\}$ (Fig. 2). The HMM state changes at each discrete time point t according to the probabilities associated with the state transitions and the current measurement/observation Z_t. The transition probabilities between states are defined in a matrix A (dimension $N \times N$) where each element a_{ij} of A is the probability that the HMM moves from state i to state j ($a_{ij} \geq 0$ and $\sum_j a_{ij} = 1$). To employ an HMM, we define an observation likelihood (observation score) $O_t(i) = P(Z_t|s_i)$. It represents the likelihood that the state s_i at time t produced the observation Z_t.

Following Rabiner et al. [20], the Viterbi algorithm selects at time t the optimal path over time (called Viterbi path) through the state space based on the maximum $\delta_t(i)$ which is the best score along a single path that starts in any state at time 0 and ends in state s_i at time t. The Viterbi algorithm takes into account the t previous system states. Starting from an initial distribution of the probabilities over the states $\Pi = \{\pi_1, \dots \pi_N\}$ where $\sum_{j=1}^{N} \pi_j = 1$, the algorithm initializes $\delta_0(i)$ as follows:

$$\delta_0(i) = \pi_i. \tag{1}$$

Next, $\delta_t(i)$ can be computed using recursion [20]:

$$\delta_t(i) = \max_j [\delta_{t-1}(j)\, a_{ji}]\, O_t(i). \tag{2}$$

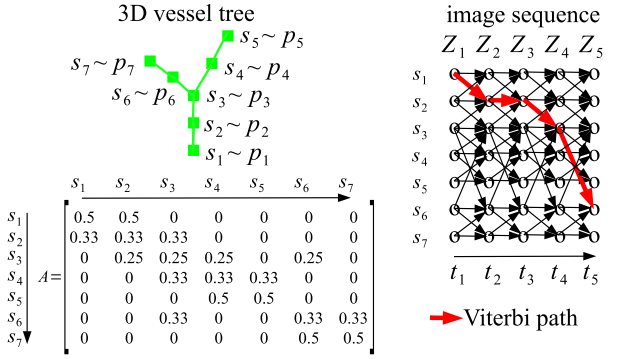

Fig. 3. HMM with a vessel tree. In this example, the transitions between possible tip locations exist only with direct neighbours and are equiprobable. The Viterbi path goes to the optimum tip position knowing the observations $Z_1 \dots Z_5$ in the 5-images sequence.

The next section explains the relation between HMM and tracking of a catheter tip in 3D using fluoroscopic images.

B. Catheter Tip Tracking

1) Timepoint: The timeline is associated with the frames of the 2D X-ray image acquisition (around 7 Hz). Each discrete time point t of the HMM corresponds to a 2D X-ray image Z_t. The measurement/observation for the HMM is the 2D X-ray image.

2) States: The 3D catheter tip is tracked inside the 3D vessel tree centerline extracted from the 3DRA. The vessel tree is discretized as a set of 3D points $P = \{p_1, \dots p_N\}$. The probability that the catheter tip is at position p_i is the probability that the HMM is in the state s_i. The function $\delta_t(i)$ is then the score that the tip is at the position p_i in the tree for the discrete time point t (Fig. 3). In our application, the liver arteries move because of respiration. For our model, we define p_i^0 the position of the 3D point p_i in the world coordinate system at time $t = 0$ (starting position at 3DRA acquisition), and p_i^t its position at time t.

3) Matrix A of State Transition Probabilities: The matrix A of state transition probabilities describes all the transition probabilities a_{ij} for the catheter tip to move from one point p_i to another point p_j in the vessel tree P (state s_i to s_j), between two time points (i.e. between two subsequent 2D X-ray images). As the interval of time is relatively short, the probabilities of transition should be high in the vicinity of the point p_i because the catheter (and so the tip) is not expected to move very far away. Therefore, the transition probabilities are set according to the distance along the vessel path between points p_i and p_j of the 3D vessel tree. Two distributions are proposed to model the catheter tip motion: one, a'_{ij}, restrictive around the point p_i and one, a''_{ij}, flexible in the close vicinity of p_i. The first one models a catheter moving relatively slow with a Gaussian function [21]:

$$a'_{ij} = e^{-\frac{D(p_i,p_j)^2}{2\sigma_a^2}} \tag{3}$$

where σ_a controls how fast and far the catheter tip can move, and where $D(p_i, p_j)$ models the distance (along the vasculature) between p_i and p_j. I.e. let $\{g_1, \dots g_n\}$ be the set of points representing the vessel centerline between the points

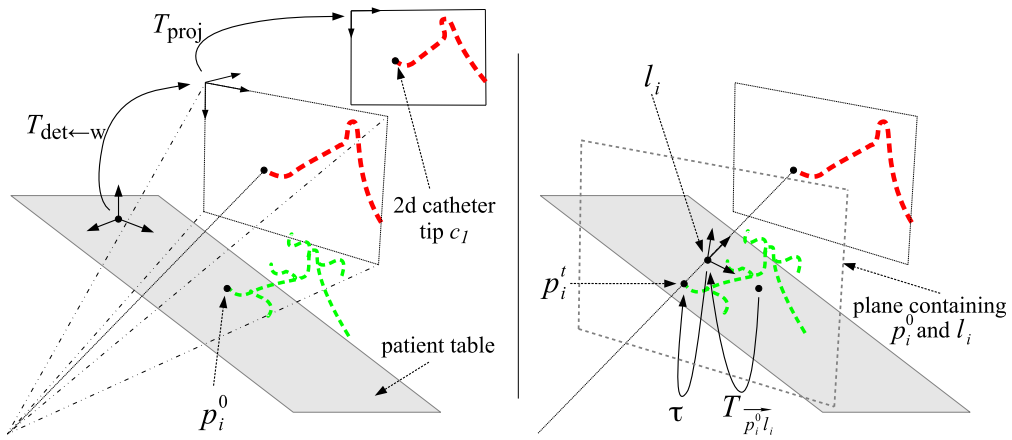

Fig. 4. Initial position of the 3D vessel tree (in green) with the 2D projected catheter (in red) at time t (left figure). 3D points are transformed from the 3D world coordinate system to the 3D X-ray detector plane coordinate system ($T_{\text{det}\leftarrow w}$) and then projected to the 2D image plane (T_{proj}). Registered position of the 3D vessel tree (knowing that the catheter tip is at the position p_i) after the computation of the optimal transformation τ (right figure).

$p_i = g_1$ and $p_j = g_n$, then $D(p_i, p_j)$ is defined as the sum of the distances between each neighboring pair g_k, and g_{k+1}:

$$D(p_i, p_j) = \sum_{k=1}^{n-1} ||g_k, g_{k+1}||. \tag{4}$$

The second distribution gives the same probability for moving to any point in the vicinity of the point p_i, where vicinity is defined by a maximum distance θ (in mm). We have $a''_{ij} = 1$ when $D(p_i, p_j) \leq \theta$ and $a''_{ij} = 0$ when $D(p_i, p_j) > \theta$. Because the matrix A defines probabilities, $\sum_j a_{ij}$ has to be equal to 1, thus we normalize the coefficients a' (resp. a'') to obtain $a_{ij} = a'_{ij} \cdot (\sum_j a'_{ij})^{-1}$ (resp. $a_{ij} = a''_{ij} \cdot (\sum_j a''_{ij})^{-1}$).

4) Observation Scores: During the tracking, for each point p_i, we need to compute the score $\delta_t(i)$ (Equation 2), showing how likely the observation is following the previous system states and under the condition that the tip is at the position p_i (the system in the state s_i) at time t. Thus each observation score (likelihood) $O_t(i)$ needs to provide information on the current state, based on the X-ray image Z_t. In our method, we evaluate the observation score via 3D/2D registration. In other words, the better the 3D/2D registration is (following our registration metric), the better the observation score will be. Each observation score $O_t(i)$ is based on the 3D/2D registration between the catheter shape extracted from the 2D X-ray image Z_t and the unique 3D catheter path centerline $V_i = \{v_1, \ldots v_{n_{V_i}}\}$, starting from the tip p_i and going to the root of the tree. The catheter shape is defined as a set of 2D points in the image coordinate system $C_t = \{c_1, \ldots c_{n_{C_t}}\}$. The observation score $O_t(i)$ is a likelihood between 0 and 1 stating how the 3D/2D registration performed at time t given that the tip is at the position p_i in the vessel tree. It is defined as a Gaussian function:

$$O_t(i) = e^{-\frac{M(C_t, V_i)^2}{2\sigma_s^2}} \tag{5}$$

where M is the metric of the 3D/2D registration and σ_s controls the scaling of the registration metric.

The 3D/2D registration between the vessel path V_i and the catheter C_t determines the transformation matrix τ that minimizes the metric M. M quantifies the alignment of the 3D vessel with every point of the 2D catheter:

$$M(C_t, V_i) = \min_{\tau} \left(\sum_{c \in C_t} F_{\text{cost}}(c, V_i, \tau) \right) \tag{6}$$

where $\tau = T_{\text{rot}_z}\, T_{\text{rot}_y}\, T_{\text{rot}_x}\, T_{\text{trans}_x}$ is a 4 degrees of freedom rigid transformation matrix (three rotations and one translation), and F_{cost} is a function that represents how close is a 2D point of the catheter to the projected 3D vessels knowing the transformation τ. The transformation τ only has 4 degrees of freedom because the projection of the 3D tip p_i^t at time t has to match the 2D catheter tip c_1 and therefore the transformation τ translates only along one axis, the line from c_1 to the origin of the X-ray projection, and rotates around it (Fig. 4).

In order to define the cost function F_{cost}, we first explain how the 3D vessel tree is projected from the world coordinate system to the image coordinate system. We compute (in the world coordinate system) the intersection of the line projecting c_1 (i.e. the line from X-ray source to c_1 on the X-ray image/detector plane) with a plane that is parallel to the image plane, and that contains the 3D tip p_i^0. This intersection is represented by the point l_i which will be the starting point as a 3D catheter tip for the registration search of τ. As any point on the line along the X-ray source projects on c_1, the only translation allowed to find p_i^t is along this line. Furthermore, the center of rotation of τ is the same point l_i, such that the rotations also guarantee that p_i^t projects on c_i. Therefore, the projection transformation is parametrized as follows (Fig. 4):

$$F_{\text{proj}}(v, \tau) = T_{\text{proj}}\, T_{\text{det}\leftarrow w}\, T_{w\leftarrow l_i}\, \tau\, T_{l_i\leftarrow w}\, T_{\overrightarrow{p_i^0 l_i}}\, v \tag{7}$$

where $T_{\overrightarrow{p_i^0 l_i}}$ is the translation along the line p_i^0 to l_i in the world coordinate system and $T_{l_i\leftarrow w}$ is the transformation from the world coordinate system to the coordinate system centered around l_i. The transformation T_{proj} is the cone-beam projection and $T_{\text{det}\leftarrow w}$ the transformation matrix from the world to the C-arm detector (X-ray image plane). Both transformations are known because of the C-arm geometry (given in the DICOM

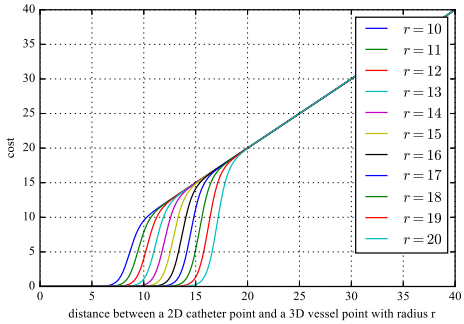

Fig. 5. F_{cost_2} in function of the distance F_{cost_1} and various radius r.

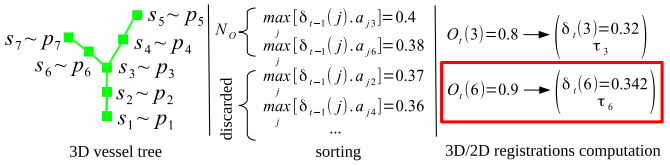

Fig. 6. Process example with $N_O = 2$. At time t, p_6 is the most likely position for the catheter tip. τ_6 is the result of the minimization for the 3D/2D registration when evaluating O_t▷6◁.

file). Because the projection of the 3D tip p_i^t is the 2D catheter tip c_1, we have $F_{\text{proj}}(p_i^t, \tau) = c_1$.

We propose two cost functions to measure how far a 2D catheter point is from a projected 3D vessel. The first one is the minimal distance between each point of the 2D catheter C_t and any projected point of the 3D centerline V_i:

$$F_{\text{cost}_1}(c, V_i, \tau) = \min_{v \in V_i} ||c - F_{\text{proj}}(v, \tau)|| \tag{8}$$

where $F_{\text{proj}}(v, \tau)$ is the projection of the 3D point v onto the 2D images. This cost function ignores the vessel diameter when registering the centerline of the vessel path V_i. As some vessels may have a large diameter (e.g. in the hepatic artery or the aorta), we defined a second cost function that takes into account the vessel diameter and reduces the cost of the alignment when the catheter is inside a vessel V_i. Using the known radiuses $R_i = \{r_1, \ldots r_{n_{V_i}}\}$ associated with every point of the vessel V_i, the second cost function based on sigmoïd is (Fig. 5):

$$F_{\text{cost}_2}(c, V_i, \tau) = \frac{F_{\text{cost}_1}(c, V_i, \tau)}{1 + e^{\alpha_1 \cdot (-F_{\text{cost}_1}(c, V_i, \tau) + \alpha_2 \cdot r)}} \tag{9}$$

where α_1 and α_2 control the cost inside the vessel and r is the radius of the point $v \in V_i$. v is the point which has the minimum distance with the catheter point c in the first cost function $F_{\text{cost}_1}(c, V_i, \tau)$. We want F_{cost_2} to start to penalize when the minimum distance reach the radius r. The variables $\alpha_1 = 2$ and $\alpha_2 = 0.85$ fit to obtain this behaviour (Fig. 5).

5) Viterbi Algorithm: For each image, the Viterbi path [20] is computed from the initial state position at the first image to the current image. This results in the most likely 3D tip point p_i for each image, and also (as a 3D/2D registration has been performed during the observation scores evaluation) the transformation τ that aligns the projected 3D vessel tree with the 2D fluoroscopy.

Theoretically, at time t, the observation score $O_t(i)$ for every state i should be evaluated. For large vessel trees, that may contain hundreds of points, this would not permit real-time use. Therefore, to reduce the computational effort, the observation scores of only a relatively small number of N_O states are evaluated and for all the other states, the observation scores are set to 0. To this end, we first sort all the states s_i following the score $\max_j[\delta_{t-1}(j)\, a_{ji}]$. The N_O states with the best scores will be selected to have their observation scores $O_t(i)$ evaluated. Thus, only the most likely tip positions will be evaluated and the other possible tip positions will be discarded (Fig. 6).

III. Experiments

The method presented in the previous section was qualitatively and quantitatively evaluated, considering the accuracy as well as the robustness. The evaluation was carried out on both simulated data and clinical data. In the following, we describe respectively the data acquisition and implementation, the simulation experiments and the experiments using clinical data.

A. Data Acquisition and Implementation

We retrospectively acquired data of 28 Transcatheter Arterial Chemoembolization (TACE) procedures. The data, which were anonymized prior to use in this study, comes from three different hospitals (Erasmus MC, University Medical Center, Rotterdam, the Netherlands; the Hôpitaux Universitaires Henri Mondor, Créteil, Paris, France; and the Ospedale di Circolo e Fondazione Macchi, Varese, Italy) using intervention rooms with angiographic C-arm systems (Xper Allura, Philips Healthcare, Best, the Netherlands). In total, we acquired 10 long fluoroscopic sequences (46-76 frames) from 10 procedures and 74 angiographic sequences (4-11 frames) from 19 procedures (one is in common with the long sequences set). A 3DRA image was acquired at the beginning of each intervention when the catheter was in the common hepatic artery. For each fluoroscopic image Z_t in each sequence (i.e. all the frames), the 2D catheter centerline C_t was manually segmented by annotating points on the 2D catheter and then fitting a continuous spline to these points. The 3D vessel tree centerline P in the 3DRA was extracted with a semi-automatic method based on thresholding and skeletonization [22]. Each point $p \in P$ is associated with the radius of the vessel at that position. The catheter C_t and the vessel tree P are discretized with a sampling distance of γ mm between every consecutive point. The effect of the sampling distances $\gamma = \{0.5, 1.5, 3, 6, 9\}$ mm is evaluated in the experiments.

To minimize the metric M, we used the Powell optimizer [23] where the rotation rot_x, rot_y and rot_z, and the translation along the projected line trans_x (from the transformation τ) are the optimization parameters. As the 3D vessel tree will translate and rotate around the projected line of the 2D catheter tip position, the initial position of the 3D vessel tree is already close to the optimal position. Thus, we can have a rather limited search space during the registration.

The rotations have been constrained between $\pm$ 2° and the translation between $\pm$2 mm. Larger rotations around rot_y and rot_z can lead to overlapping vessels and less reliable registrations.

When the HMM updates $\delta_t(i)$ are computed, values can become very small over the time and as a result, computations may be numerically unstable. As Rabiner et al. [20] suggest, updates can also be computed in log scale in order to get numerical results more stable. The equation in log scale becomes:

$$\delta_t(i) = \max_j[\delta_{t-1}(j) + log(a_{ji})] + log(O_t(i)) \tag{10}$$

The experiments were run on an laptop Intel Core i7 (2 Ghz). The HMM tracking method source code is available.[1]

B. Patient Vessel Tree With a Moving Simulated Catheter

We performed experiments on simulated data; the main purpose of these experiments was to apply and evaluate the tracking algorithm in the context of data with ground truth. With this simulation, we know the exact position of the 3D catheter and the 3D vessel tree, with respect to the C-arm system. We thus can project the simulated catheter and obtain the position of the 2D simulated catheter. Then, similar to the real data scenario, the algorithm tracks the 3D catheter tip position in the 3D vasculature (using the 3D vessel tree centerline, the 2D catheter centerline at each frame and the first 3D tip position to initialize the distribution of the probabilities over the states: Π). Below, we first describe how the simulation data was generated, and then we detail the experiments running these data.

1) Catheter Simulation: To obtain realistic data, a 3D catheter is simulated using the clinical data i.e. 3D vessel tree and fluoroscopic image projection. In the simulation, we included catheter motion inside the vasculature and respiration induced motion. This was done as follows: For each fluoroscopic sequence, the 3D vessel tree (extracted from the 3DRA) was manually registered with a frame where the 2D catheter tip is at the most distal position in the vasculature in order to get the longest catheter visible. The goal is not to obtain an accurate registration but a simulation as close as the real clinical case. Because of the manual registration, the catheter tip position in the 3D vessel tree is obtained. A catheter is generally not at the vessel center, but rather positioned at the boundaries of the vessels. So, from the tip position, an initial catheter shape is determined by extracting a minimum cost path inside the vessel tree binary mask from the catheter tip position to the root of the vessel tree; the resulting path is the simulated catheter C_m. The catheters $C_0, C_1, \ldots, C_{m-1}$ are constructed from C_m. The catheter and thus the tip move from the hepatic artery, where the contrast agent has been injected during the 3DRA acquisition, to the tip position of C_m. The displacement has a fixed speed for each sequence, randomly chosen in a range from 1 to 10 mm/frame. C_0 is the first catheter shape, running from the root until the hepatic artery. $C_1, \ldots, C_{m-1}$ are similar parts of C_m, always starting at the root and ending at a position in-between the hepatic artery and the tip position of C_m. These positions are computed such that the catheter tip advances with a fixed speed. A Gaussian smoothing with a random $\sigma \in [1, 2]$ mm is applied on every constructed catheter to add a slight deformation. Additionally, the catheter motion caused by respiration is simulated by translating the catheter in the cranial-caudal direction. The translation amplitude is defined as:

$$\text{translation}(i) = \lambda \sin\left(\frac{2\pi}{\beta} i\,\Delta_t\right) \tag{11}$$

where $\lambda = 10$ mm is the peak amplitude, $\beta = 4$ s the respiration period, i the number of the current image in the sequence and $\Delta_t = 0.133$ s the time between two images, obtained from the clinical fluoroscopic image frequency.

2) Experiments and Parameters Optimization: The catheter simulation is based on the 74 angiographic sequences. 6 sequences have been discarded because the catheter was too short (less than 8 cm) to simulate a tip motion. The sequences with catheter simulation are divided in one training set with 20 sequences originating from 7 procedures and one test set with 48 sequences originating from 12 different procedures. First, experiments have been done to choose optimal parameters. We used the simulated catheters to evaluate the tracking accuracy. To this end, we computed the 3D distance between the ground truth catheter tip and the tip after the registration for each frame of each simulated sequence. For each experiment, the two cost functions (F_{cost_1} and F_{cost_2}), and the two transition distributions (a' and a'') were evaluated.

The parameters σ_a and θ from the transition matrix A, and σ_s from the observation score were optimized with the training set. The purpose is to evaluate the tip tracking accuracy of the method as a function of σ_a, θ and σ_s and therefore we report the 3D tip distance over all the frames of sequences. The parameter values that gave the shortest median distance were used for all the following experiments. The evaluation has been done with the values: $\sigma_a = \{6, 9, 12, 15, 18, 20\}$ mm, $\theta = \{6, 9, 12, 15, 18, 20\}$ mm and $\sigma_s = \{0.25, 0.5, 1, 1.5, 2, 2.5\}$ mm. For these experiments, the sampling γ of the 2D catheter and the 3D vessel tree centerline is set to 3 mm and the number of observation scores to evaluate N_O is set to 200.

The sampling γ and the number of observation scores to evaluate, N_O, affect computation time, and may also affect method accuracy. We investigated the effect of using different samplings γ and different N_O with the optimal values of θ, σ_s, the cost function F_{cost_1} and the transition distributions a'' (determined for each sampling γ and $N_O = 200$, like the previous experiment). The samplings $\gamma = \{0.5, 1.5, 3, 6, 9\}$ mm and $N_O = \{10, 25, 50, 100, 200\}$ have been evaluated. The 3D distance between the real and registered tip is reported to find the optimal accuracy/computation time tradeoff.

With the optimal parameters, the test set is evaluated and the 3D tip distance is reported. Also, the robustness of the tracking was evaluated by determining whether the catheter tip is tracked correctly until the end of the sequence; we consider a tracking failed when the registration results of the last 5 images of the sequence yield a 3D distance between the real catheter tip and the registered one greater than 3 mm. The percentage of tracking failures is reported.

[1] https://github.com/pambros/HMM-3D-Catheter-Tip-Tracking

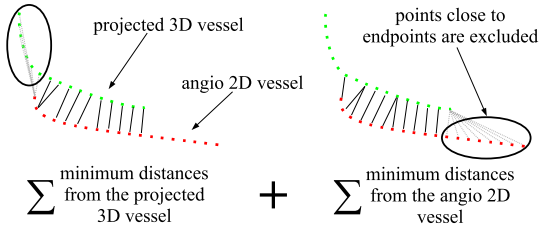

Fig. 7. Closest corresponding points distance between paired vessels used for the sequences with contrast agent evaluation.

C. Clinical Data

The optimal parameters computed with simulated catheters were used in the experiments with clinical data. As clinical data is missing ground truth for tip tracking, we conducted two different experiments:

1) One experiment with quantitative evaluation on sequences with contrast agent: 74 sequences (between 1 and 2 s length) where the catheter is not advanced significantly and the contrast agent is visible. The main motion to be recovered is the motion of the liver caused by respiration. The 2D enhanced vessels close to the tip were compared with the 2D vessels projected from the 3D vessels tree.
2) One experiment with qualitative evaluation on motion sequences: 10 sequences where the catheter is advanced (between 7 and 10 s length). The tracking was visually checked.

For each sequence, in the first frame, the 3D tip is manually annotated in the 3D vessel tree to initialize the method. Although annotating the exact position is difficult, the annotation is sufficient for the initialization of the HMM. If the point p_i is the manual 3D tip position annotation, then π_i is set to 1 and all the other position probabilities in the initial distribution Π are set to 0.

1) Experiments With Sequences With Contrast Agent: Angiographies or DSA were acquired for the sequences with contrast agent. The last X-ray images of the sequences show the vasculature in the vicinity of the tip of the catheter. These vessels can be compared with the 2D projection of the 3D registered vessel tree. We used the same evaluation as described in our previous method [17]. The evaluation metric is the average distance of the closest points between the 2D vessels and the 2D projection of their corresponding 3D vessels (Fig. 7). The correspondence between the projections of the 3D vessels and the 2D vessels in the angiographies is unknown. Therefore, we manually paired the vessels visible in the X-ray angiography to the vessels projected from the 3D tree (Fig. 8). The distances between the paired vessels close to the tip are then computed. The most relevant region for the tip tracking is the area close to the catheter tip; we therefore only evaluated in a circular region (3 cm radius) around the catheter tip. The 2D vessels from the angiographies are manually segmented and the 3D vessel tree is projected onto the image using the C-arm geometry. In order to help the visual pairing, the 2D projection of the 3D vessel tree was manually aligned, this alignment was not used in the tracking experiments.

TABLE I
OPTIMAL SETTINGS RESULTING FROM THE SIMULATED EXPERIMENTS. THE BOLD LINE IS THE OPTIMAL ONE

Transition distribution	σ_a	θ	Registration cost function	σ_s	N_O	Sampling γ
a'	9 mm	N/A	F_{cost_1}	0.25 mm	25	3 mm
a'	12 mm	N/A	F_{cost_2}	0.25 mm	25	3 mm
$\boldsymbol{a''}$	**N/A**	**9 mm**	$\boldsymbol{F_{\text{cost}_1}}$	**0.25 mm**	**25**	**3 mm**
a''	N/A	18 mm	F_{cost_2}	0.25 mm	25	3 mm

2) Experiments With Motion Sequences: The method is applied on every sequence and the tracking results are evaluated visually. For each second of each sequence, we report one of the three following observations: "Correct tracking", "Incorrect tracking but clinically relevant", "Incorrect tracking and no clinical relevance". Clinical relevancy means that the the 2D projected roadmapping of the vasculature still gives useful visual information.

During the procedure, the physician regularly moves the table and the C-arm detector, and changes magnification or the field of view. Most of the time, when the catheter is closer to the tumor, the field of view is centered at the tip of the catheter. In those cases, only the distal part of the catheter is visible and the registration is challenging. To evaluate the tracking method also in those cases, for each fluoroscopic sequence, part of the proximal segmented catheter centerline was removed. At one third (resp. two third) of the sequence, 33% (resp. 66%) of the segmented catheter is removed. The visual evaluation of the tracking method on these sequences with field of view simulation is reported.

IV. RESULTS

A. Patient Vessel Tree With a Moving Simulated Catheter

Figure 9 shows the tracking results of the simulated training set with the two cost functions (F_{cost_1} and F_{cost_2}), the two transition distributions (a' and a''), and for various σ_a, θ and σ_s. The median distance between the 3D tip and the 3D registered tip is below 2.6 mm for more than half of the experiments (67%) with the cost function F_{cost_1}. Results with the transition distribution a'' have a median distance smaller than those with the distribution a' except for a few experiments (4%). For the following experiments, we choose the optimal settings with the experiments giving the shortest median distance. Table I summarizes the chosen parameters. The experiment could have been done with σ_s smaller than 0.25 mm to check if the median distance would decrease. However, the pixel size of the fluoroscopic sequences is on average 0.23 mm and thus a smaller σ_s would be beyond the pixel resolution, and the accuracy of the catheter centerline extraction. The cost function F_{cost_1} and the transition distribution a'' were chosen for the subsequent experiments. Though the median distance is similar for both transition distribution a' and a'', a'' is less sensitive to the parameter settings σ_s and θ. Additionally, the implementation of F_{cost_1} and a'' is also simpler and the computation time is lower.

The optimal settings have also been computed for the samplings $\gamma = \{0.5, 1.5, 6, 9\}$ mm with $N_O = 200$, cost function F_{cost_1} and transition distribution a''. For all the

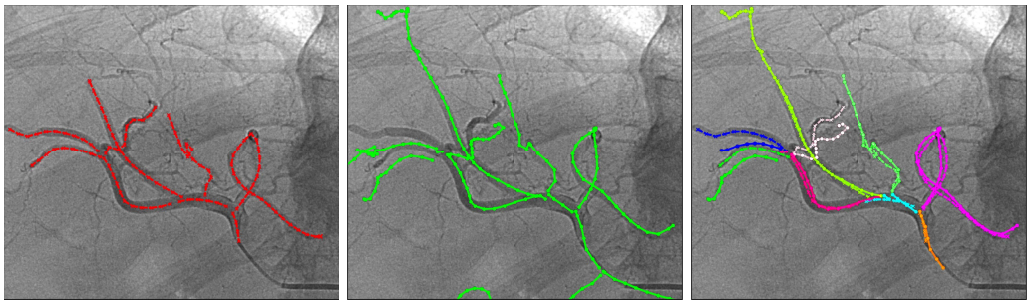

Fig. 8. Annotation example for the sequences with contrast agent evaluation: 2D segmented vasculature from contrast agent (left), 2D projection of 3DRA vasculature after manual registration (center) and manual paired vessels used for the evaluation (right). The paired vessels (between the 2D vasculature and the 2D projection of 3DRA vasculature) are presented in the same color.

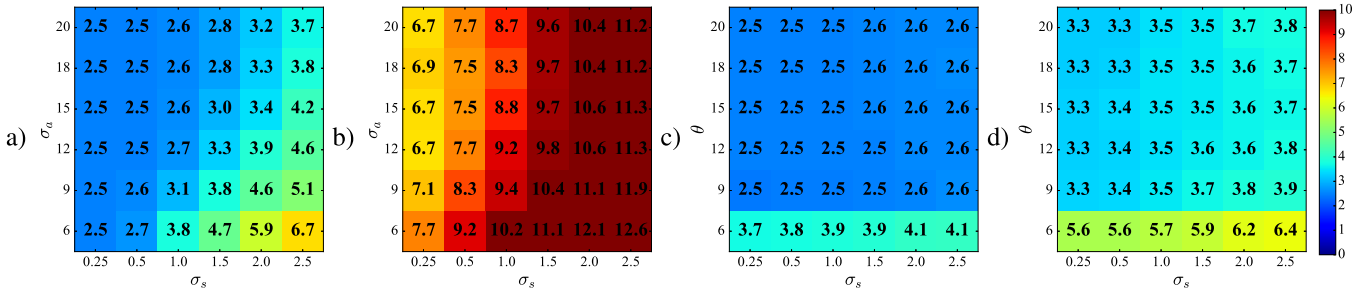

Fig. 9. Median distance between the 3D tip and the 3D registered tip (in mm) for each frame of the simulated sequence training set with different σ_a, θ and σ_s (in mm). Experiments with the cost function F_{cost_1} and the transition distribution a' (a), with F_{cost_2} and a' (b), with F_{cost_1} and a'' (c), with F_{cost_2} and a'' (d).

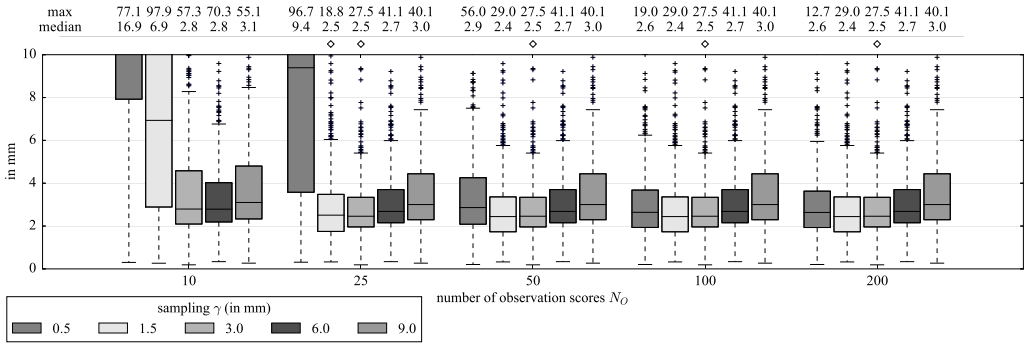

Fig. 10. Distance between the 3D tip and the 3D registered tip (in mm) for each frame of the simulated sequence training set with different samplings γ (in mm), number of observation scores N_O and optimal settings ($\theta = 9$ mm, $\sigma_S = 0.25$ mm, F_{cost_1} and a''). $\diamond$ indicates that there is no statistically significant difference (p-value > 0.05 with a Wilcoxon signed-rank test) between this experiment and the experiment with optimal settings (with $\gamma =$ 3 mm sampling and N_O $\mathcal{D}$ 25). The boxes of the boxplot report first and third quartiles, and median values. The whiskers report $\pm$ 1.5 times the inter-quartile range around the box.

samplings γ, we obtain the optimal settings $\theta = 9$ mm and $\sigma_s = 0.25$ mm. With these settings, the impact of the centerlines sampling γ and the number of observation scores N_O is shown in Figure 10. The experiments with the sampling $\gamma = 1.5$ and 3 mm obtain the smallest median distances (less than 2.5 mm) and standard deviations, with a number of observation scores N_O greater than 50, and greater than 25 for the 3 mm sampling. The average registration time is less than 53 ms for all the experiments with a sampling greater than 3 mm (Fig. 11). For all the following experiments, the 3 mm sampling and $N_O = 25$ are chosen as a tradeoff between accuracy, robustness and computation time (see Table I).

Figure 12 shows the distance between registered tip and real tip during the tracking with the test set and optimal settings. With the settings that result from the previous experiments and the definition described in the "Experiments and parameters optimization" section, the tip tracking failed to reach the last tip position in less than 16.7% of the sequence test set.

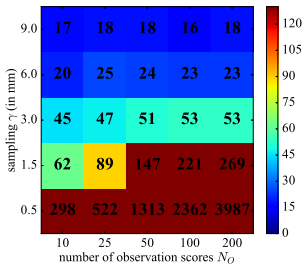

Fig. 11. Average registration time (in ms) for each frame of the simulated training set with different samplings γ (in mm) and number of observation scores N_O.

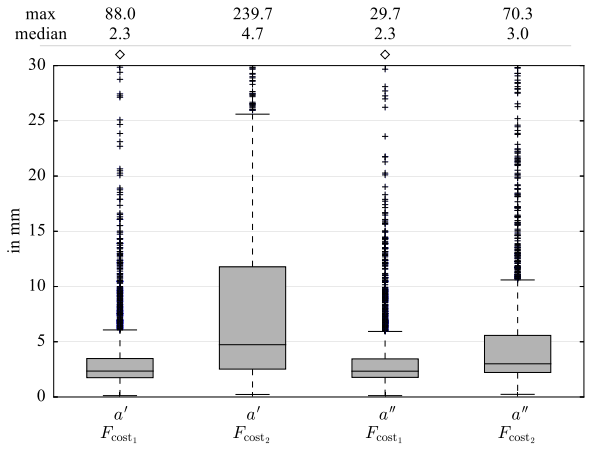

Fig. 12. Distance between the 3D tip and the 3D registered tip (in mm) for each frame of the simulated sequence test set with the optimal settings (see Table I). $\diamond$ indicates that there is no statistically significant difference (p-value $>$0.05 with a Wilcoxon signed-rank test) between this experiment and the experiment with optimal settings (cost function F_{cost_1} and transition distribution a''). The boxes of the boxplot report first and third quartiles, and median values. The whiskers report $\pm$ 1.5 times the inter-quartile range around the box.

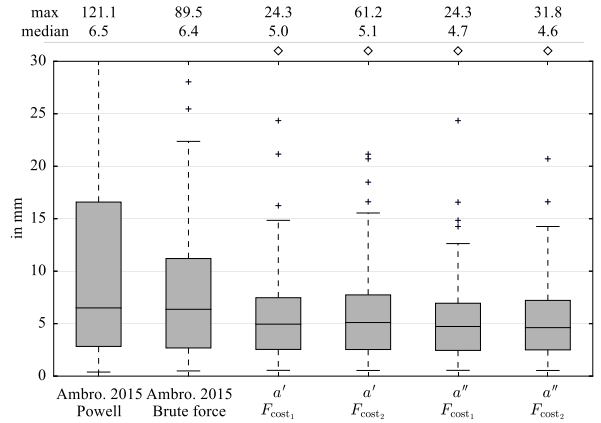

Fig. 13. Average distance between paired vessels (within 3 cm radius from the tip) for each sequence with contrast agent after registration (in mm). The optimal settings were used (see Table I). $\diamond$ indicates that there is no statistically significant difference (p-value $>$0.05 with a Kruskal-Wallis test) between this experiment and the experiment with optimal settings (cost function F_{cost_1} and transition distribution a''). Kruskal-Wallis test has been used because we do not have paired samples (number of paired vessels can differ following the tip position). The boxes of the boxplot report first and third quartiles, and median values. The whiskers report $\pm$ 1.5 times the inter-quartile range around the box.

B. Clinical Data

Figure 13 shows the average distance between paired vessels (within 3 cm radius from the tip) for all the sequences with contrast agent after the tracking and registration. The optimal settings are used and the two cost functions and two transition distributions are evaluated. We also compare with our previous method [17]. The transition distribution a'' with the cost function F_{cost_2} gives the lowest median average distance (4.6 mm) but there is no statistically significant difference (p-value $>$0.05 with a Kruskal-Wallis test) between the different transition distributions and cost functions. Our previous none-tracking method yielded a larger median average distance and the distribution is wider as well. The average computation time of the previous method is 236 ms with Powell optimizer and 5.2 s with brute force. The four combined tracking methods have an average computation time of 64 ms.

The tracking method with optimal settings (see Table I) has been applied on the original 10 motion sequences and on the 10 motion sequences with field of view simulation (part of the catheter removed) (Fig. 14). Tracking results based on visual observations are depicted in Figure 15. Two video clips showing the tracking results are available as supplementary material.[2] The 3D vasculature (in green) is projected on the fluoroscopy and only the vessel branches after and in the vicinity of the catheter tip are displayed. The tip tracking is on average visually correct on eight motion sequences (Fig. 15). "Incorrect tracking but clinically relevant" means that the tip tracking is incorrect but the 2D projected roadmapping of the vasculature still gives useful visual information. For example, in the end of the sequences 9 and 10, the tracked tip is shifted or enters the wrong vessel but the resulted registration can still be used as a roadmap. In sequence 9, the tracked tip enters in a loop-shaped vessel parallel to the correct path. In sequence 10, the 3DRA image has to be rotated significantly (at least 10° around the cranial-caudal axis) from its initial position to fit with the catheter position. The limited search space during the 3D/2D registration prevents the optimizer to reach the correct fit and therefore the tracking tip is not very smooth. Sequences 3 and 6 have the same problem but also have a catheter shape which is considerably deformed compared to the vessel shape in the 3DRA image. The conclusions for the tracking with the simulated field of view are the same, except for sequence 8 at eight seconds, where the remaining simulated catheter part is short. In this case, the lack of discriminative shape information in the remaining visible part of the catheter prevents to have a correct 3D/2D registration. On the other hand, in sequence 3 (compared to the tracking with unaltered motion sequences), after four seconds, the simulated field of view is helping the tracking because the beginning of the catheter is not visible and this part is actually difficult to align due to its large deformation compared to the vessel extracted from the 3DRA. Here we note that the HMM method mainly kept two different tracking paths more than 3 cm apart. The tracking in the first four seconds is in the wrong path and as soon as the score is getting higher in the correct path, the tracking switches immediately to this one.

V. Discussion and Conclusion

We proposed a method to track the tip of catheter in the 3D vasculature (extracted from 3DRA) that uses an HMM to model the catheter tip probabilities, and 2D catheter sequences (manually segmented from 2D catheterization single-plane fluoroscopic images). In the HMM, every 3D position in the 3D blood vessel is associated with the probability that the catheter tip is at that position; additionally we model the transitions for the catheter to move from that 3D position to a different one.

[2]Two video clips are available as supplementary downloadable material at http://ieeexplore.ieee.org (This material is 61.3 MB in size).

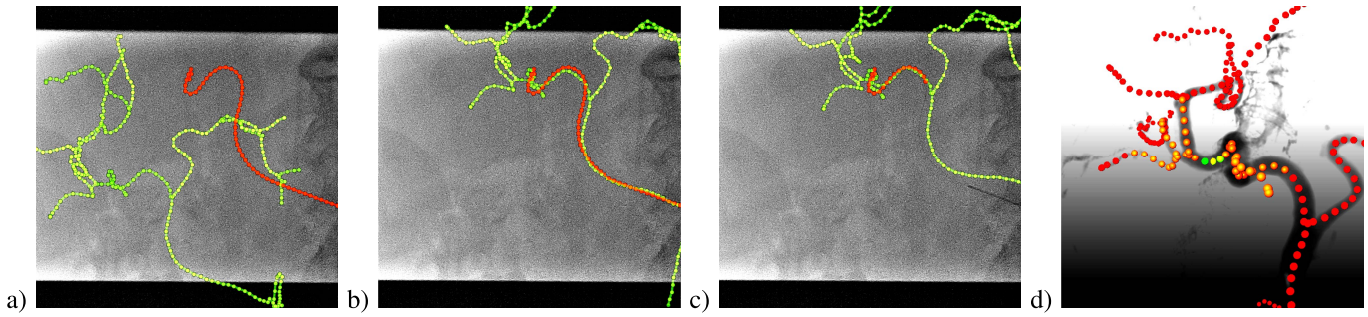

Fig. 14. Tip tracking with the catheter (in red) and the projection of the vessel tree (in green). Before the tracking with 3DRA at its initial position (a), breathing and table motion are the causes for the misalignment. After the tracking (b). After the tracking with the simulated field-of-view (shorter catheter visible) (c). Tracking in the 3D view (d), from a different angle than the projection, with the colored score δ_t for every point (scale between red (score = 0) and green (best score).

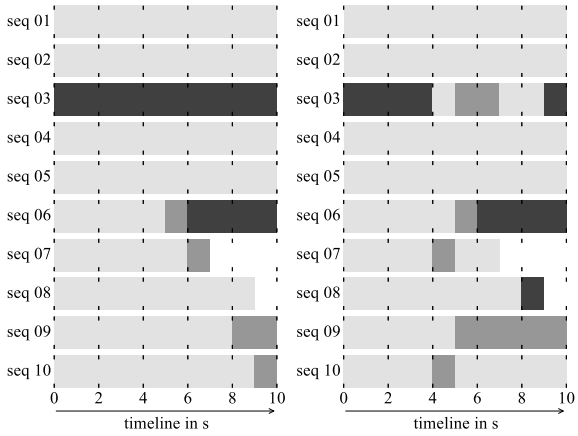

Fig. 15. Visually-based observations of the tip tracking over time for the 10 motion sequences: tracking of the unaltered sequences (left) and tracking of the sequences with field of view simulation (right). For each second of the trackings, we attribute one of the three following observations: "Correct tracking" (light gray), "Incorrect tracking but clinically relevant" (dark gray) and "Incorrect tracking and no clinical relevance" (black).

With the optimal settings, the simulated catheter results have a median 3D distance of 2.3 mm between the real-tip and the registered tip position. The results of the experiments with simulated catheters show that a transition matrix with constant probabilities (a'') is less sensitive to parameter changes (we obtain a smaller median distance with most of the parameters) than when using Gaussian distributed transition probabilities (a'). This may be explained by the fact that in case of constant transition probabilities, the probabilities derived from the registration cost function are more discriminative and thus will lead to select the best registration instead of choosing a less well registered one because that one has a higher prior probability due to the non-constant transition matrix. In the simulated catheter experiments, the error is larger with the cost functions F_{cost_2} (taking into account the radius) than with F_{cost_1}. The cost function F_{cost_2} apparently does not constrain the catheter/vessels alignment sufficiently, which may lead to an inaccurate tip position. The catheter and vessel deformation simulation may also be insufficiently realistic to demonstrate added-value of taking into account the vessel diameter during the registration.

The number of observation scores N_O is directly related to the discretization γ of the 3D vessel tree and the 2D catheter. Intuitively, if the sampling γ is denser, the number of observation scores N_O must be increased to maintain similar results. This assumption is verified with the experiments. The accuracy and the robustness of the tip tracking are optimal when the vessels and the catheter are sampled with γ = 3 mm (resp. 0.5 or 1.5 mm), and the number of observation scores to evaluate N_O is more than 25 (resp. 50 or 200). In our case, a sampling of γ = 3 mm and $N_O = 25$ provide a reasonable tradeoff for real-time registration.

The experiments with clinical data with a catheter that is not advanced, and where contrast agent is introduced, yield a median average distance between paired vessels of 4.7 mm using optimal settings. Here, both cost functions F_{cost_1} and F_{cost_2} have similar results. The deformations of vessels and catheter in clinical data are much larger than our simulated data, therefore the registration cost function F_{cost_2} which takes the radius into account is probably more effective than with simulated catheters.

The curvature of the vasculature and catheter is relevant in the tracking. A unique catheter shape (with high curvature) originating from a unique shape of the vasculature will facilitate the registration. In our previous method [17] we propose a method based solely on the catheter shape. The tracking was generally successful in cases with a unique catheter shape but our experiments also demonstrated that the registration can fail when the shape is not sufficiently discriminant. The tip tracking in our current method enables a more robust registration when the catheter has a simple shape or is rather short.

The tracking and the associated 2D or 3D roadmap can be used for guidance to navigate the catheter through vasculature, without additional contrast agent injections. According to our clinical partners, a median vessel distance error of 4.7 mm is sufficient for them to localize the instrument in the vessel tree, and helps them guiding the catheter to the correct location. In practice, for the physicians, consistency in tip tracking is more important for guidance than the actual vessel position around the tip. Also, the experiments with clinical data with the catheter being advanced, demonstrated that the tracking is robust even when the tracking is lost for some time or when only a short part of the catheter is visible. Although the lack of a reference standard for these cases prevents us from quantifying the results, the tracking and resulting roadmap

provide visual information which may help physicians to maneuver the catheter more efficiently, and possibly to use less contrast agent. Future clinical studies need to be conducted to validate this assumption.

Most of the methods in the literature register a 3D preoperative image with 2D X-ray contrast enhanced images. Some of them obtain submillimeter accuracy. We cannot directly compare our results with those methods because we use 2D fluoroscopic images with no contrast in which only the catheter is visible, making it a much more challenging task. In order to compensate the breathing motion, Atasoy et al. [18] updated the initial 3D vasculature position using also only a small part of the catheter (extracted in a manually selected region of the X-ray image). They evaluated on one clinical sequence by computing the overlap of the catheter with the vasculature, resulting in 70% overlap. Our tracking method with the motion sequences obtains on average 80.3% overlap. However, this evaluation metric does not give information about the catheter tip and the vessels around the tip.

To apply this method in the angiography suite, the 2D segmentation of the catheter has to be done automatically during each 2D X-ray frame. This task is challenging but it has been already addressed in several studies, such as Heibel et al. [24]; they demonstrated a catheter tracking accuracy of less than 1.5 pixels on liver catheterization fluoroscopic sequences. Such accuracy should be sufficient for application in clinical practice. Other methods propose to track the catheter in fluoroscopic images such as [25]–[27]. The 2D catheter detection as well as the 2D tip detection are important because the registration is solely based on the catheter centerline. We did not evaluate the error resulting from a missing tip part. However, given our approach, we expect that a missing tip part will result in an additional tip position error (in 3D) of approximately the length of the missing part. On the other hand, the roadmap should still be correct and could still help the physician to guide the catheter. In addition, the catheter tip position in the 3D vessel tree needs to be initialized once, after the 3DRA acquisition, by manually indicating the tip. This task is simple and fast, and could also be automated because the catheter can be easily identified in 3DRA.

Our method could be extended in several directions. A non-uniform sampling of the catheter and the vessel tree centerline could be used to guide the optimizer during the registration to align features such as high-curvature regions. The matrix A of state transition probabilities could similarly be adapted, e.g. at region of high curvature and also branching points. In the liver, as motion of the vessels is mainly due to respiration, the motion transformation should be small between each frame and a periodic respiratory motion is expected. It could be useful to include a motion prior in the registration transformation model.

To conclude, we presented a 3D catheter tip tracking method using an HMM with 2D fluoroscopic sequence and 3DRA. Experiments on simulated data demonstrated a median tip tracking distance error of up to 2.3 mm. On clinical data, the results demonstrate a robust tracking in cases where the catheter is advanced. In case of no advancement of the catheter, the registration yields a median distance error of less than 4.7 mm on vessels close to the tip. These accuracies indicate that the method could become a promising tool for improving image guidance in liver catheterization procedures.

ACKNOWLEDGMENT

We thank the Hôpitaux Universitaires Henri Mondor, Créteil, Paris, France and the Ospedale di Circolo e Fondazione Macchi, Varese, Italy for providing image datasets.

REFERENCES

[1] D. Ruijters, R. Homan, P. Mielekamp, P. Van de Haar, and D. Babic, "Validation of 3D multimodality roadmapping in interventional neuroradiology," *Phys. Med. Biol.*, vol. 56, no. 16, p. 5335, 2011.

[2] B. Bapst, M. Lagadec, R. Breguet, V. Vilgrain, and M. Ronot, "Cone beam computed tomography (CBCT) in the field of interventional oncology of the liver," *CardioVascular Intervent. Radiol.*, vol. 39, no. 1, pp. 8–20, 2015.

[3] P. Markelj, D. Tomaževic, B. Likar, and F. Pernuš, "A review of 3D/2D registration methods for image-guided interventions," *Med. Image Anal.*, vol. 16, no. 3, pp. 642–661, 2012.

[4] R. Liao, L. Zhang, Y. Sun, S. Miao, and C. Chefd'Hotel, "A review of recent advances in registration techniques applied to minimally invasive therapy," *IEEE Trans. Multimedia*, vol. 15, no. 5, pp. 983–1000, Aug. 2013.

[5] D. Ruijters, B. M. T. H. Romeny, and P. Suetens, "Vesselness-based 2D–3D registration of the coronary arteries," *Int. J. Comput. Assist. Radiol. Surg.*, vol. 4, no. 4, pp. 391–397, 2009.

[6] D. Rivest-Henault, H. Sundar, and M. Cheriet, "Nonrigid 2D/3D registration of coronary artery models with live fluoroscopy for guidance of cardiac interventions," *IEEE Trans. Med. Imag.*, vol. 31, no. 8, pp. 1557–1572, Aug. 2012.

[7] C. Metz *et al.*, "Alignment of 4D coronary CTA with monoplane X-ray angiography," in *Augmented Environments for Computer-Assisted Interventions*. New York, NY, USA: Springer, 2012, pp. 106–116.

[8] N. Baka *et al.*, "Statistical coronary motion models for 2D + t/3D registration of X-ray coronary angiography and CTA," *Med. Image Anal.*, vol. 17, no. 6, pp. 698–709, 2013.

[9] N. Baka, C. Metz, C. Schultz, R. van Geuns, W. Niessen, and T. van Walsum, "Oriented Gaussian mixture models for non-rigid 2D/3D coronary artery registration," *IEEE Trans. Med. Imag.*, vol. 33, no. 5, pp. 1023–1034, May 2014.

[10] J. H. Hipwell *et al.*, "Intensity-based 2-D-3-D registration of cerebral angiograms," *IEEE Trans. Med. Imag.*, vol. 22, no. 11, pp. 1417–1426, Nov. 2003.

[11] U. Mitrović, Z. Špiclin, B. Likar, and F. Pernuš, "3D-2D registration of cerebral angiograms: A method and evaluation on clinical images," *IEEE Trans. Med. Imag.*, vol. 32, no. 8, pp. 1550–1563, Aug. 2013.

[12] H. Sundar, A. Khamene, C. Xu, F. Sauer, and C. Davatzikos, "A novel 2D–3D registration algorithm for aligning fluoro images with 3D pre-op CT/MR images," *Proc. SPIE*, vol. 6141, p. 61412K-1–61412K-7, Mar. 2006.

[13] I. M. J. van der Bom, S. Klein, M. Staring, R. Homan, L. W. Bartels, and J. P. W. Pluim, "Evaluation of optimization methods for intensity-based 2D–3D registration in X-ray guided interventions," *Proc. SPIE*, vol. 7962, p. 796223, Mar. 2011.

[14] J. Jomier, E. Bullitt, M. van Horn, C. Pathak, and S. R. Aylward, "3D/2D model-to-image registration applied to TIPS surgery," in *Medical Image Computing and Computer-Assisted Intervention*. New York, NY, USA: Springer, 2006, pp. 662–669.

[15] M. Groher, D. Zikic, and N. Navab, "Deformable 2D–3D registration of vascular structures in a one view scenario," *IEEE Trans. Med. Imag.*, vol. 28, no. 6, pp. 847–860, Jun. 2009.

[16] R. Liao, Y. Tan, H. Sundar, M. Pfister, and A. Kamen, "An efficient graph-based deformable 2D/3D registration algorithm with applications for abdominal aortic aneurysm interventions," in *Medical Imaging and Augmented Reality*. New York, NY, USA: Springer, 2010, pp. 561–570.

[17] P. Ambrosini, D. Ruijters, W. J. Niessen, A. Moelker, and T. van Walsum, "Continuous roadmapping in liver TACE procedures using 2D–3D catheter-based registration," *Int. J. Comput. Assist. Radiol. Surg.*, vol. 10, no. 9, pp. 1357–1370, 2015.

[18] S. Atasoy *et al.*, "Real-time respiratory motion tracking: Roadmap correction for hepatic artery catheterizations," *Proc. SPIE*, vol. 6918, p. 691815, Mar. 2008.
[19] Y. Ma *et al.*, "Clinical evaluation of respiratory motion compensation for anatomical roadmap guided cardiac electrophysiology procedures," *IEEE Trans. Biomed. Eng.*, vol. 59, no. 1, pp. 122–131, Jan. 2012.
[20] L. Rabiner, "A tutorial on hidden Markov models and selected applications in speech recognition," *Proc. IEEE*, vol. 77, no. 2, pp. 257–286, Feb. 1989.
[21] P. Ambrosini, I. Smal, D. Ruijters, W. J. Niessen, A. Moelker, and T. van Walsum, "3D catheter tip tracking in 2D X-ray image sequences using a hidden Markov model and 3D rotational angiography," in *Augmented Environments for Computer-Assisted Interventions*. New York, NY, USA: Springer, 2015, pp. 38–49.
[22] D. Selle, B. Preim, A. Schenk, and H. O. Peitgen, "Analysis of vasculature for liver surgical planning," *IEEE Trans. Med. Imag.*, vol. 21, no. 11, pp. 1344–1357, Nov. 2002.
[23] M. J. D. Powell, "An efficient method for finding the minimum of a function of several variables without calculating derivatives," *Comput. J.*, vol. 7, no. 2, pp. 155–162, 1964.
[24] H. Heibel, B. Glocker, M. Groher, M. Pfister, and N. Navab, "Interventional tool tracking using discrete optimization," *IEEE Trans. Med. Imag.*, vol. 32, no. 3, pp. 544–555, Mar. 2013.
[25] M. G. Wagner, C. M. Strother, and C. A. Mistretta, "Guidewire path tracking and segmentation in 2D fluoroscopic time series using device paths from previous frames," *Proc. SPIE*, vol. 9784, p. 97842B, Mar. 2016.
[26] P. Wang, T. Chen, Y. Zhu, W. Zhang, S. Zhou, and D. Comaniciu, "Robust guidewire tracking in fluoroscopy," in *Proc. IEEE Conf. Comput. Vis. Pattern Recognit.*, Jun. 2009, pp. 691–698.
[27] G. Slabaugh, K. Kong, G. Unal, and T. Fang, "Variational guidewire tracking using phase congruency," in *Medical Image Computing and Computer-Assisted Intervention*. New York, NY, USA: Springer, 2007, pp. 612–619.